Washington University in St. Louis

Washington University Open Scholarship

All Computer Science and Engineering Research

Computer Science and Engineering

Report Number: WUCSE-2010-11

2010

Global Constructive Optimization of Vascular Systems

Manfred Georg, Tobias Preusser, and Horst K. Hahn

We present a framework for the construction of vascular systems based on optimality principles of theoretical physiology. Given the position and flow distribution of end points of a vascular system, we construct the topology and positions of internal nodes to complete the vascular system in a realistic manner. Optimization is driven by intravascular volume minimization with constraints derived from physiological principles. Direct optimization of a vascular system, including topological changes, is used instead of simulating vessel growth. A good initial topology is found by extracting key information from a previously optimized model with less detail. This technique is used... Read complete abstract on page 2.

Follow this and additional works at: https://openscholarship.wustl.edu/cse_research

Part of the Computer Engineering Commons, and the Computer Sciences Commons

Recommended Citation

Department of Computer Science & Engineering - Washington University in St. Louis
Campus Box 1045 - St. Louis, MO - 63130 - ph: (314) 935-6160.

Global Constructive Optimization of Vascular Systems

Manfred Georg, Tobias Preusser, and Horst K. Hahn

Complete Abstract:

We present a framework for the construction of vascular systems based on optimality principles of theoretical physiology. Given the position and flow distribution of end points of a vascular system, we construct the topology and positions of internal nodes to complete the vascular system in a realistic manner. Optimization is driven by intravascular volume minimization with constraints derived from physiological principles. Direct optimization of a vascular system, including topological changes, is used instead of simulating vessel growth. A good initial topology is found by extracting key information from a previously optimized model with less detail. This technique is used iteratively in a multi-level approach to create a globally optimized vascular system. Most of this work was completed at Fraunhofer MeVis during the summer of 2004.

Washington
University in St.Louis

SCHOOL OF ENGINEERING
& APPLIED SCIENCE

2010-11

Global Constructive Optimization of Vascular Systems

Authors: Manfred Georg, Tobias Preusser, and Horst K. Hahn

Corresponding Author: mgeorg@cse.wustl.edu

Abstract: We present a framework for the construction of vascular systems based on optimality principles of theoretical physiology. Given the position and flow distribution of end points of a vascular system, we construct the topology and positions of internal nodes to complete the vascular system in a realistic manner. Optimization is driven by intravascular volume minimization with constraints derived from physiological principles. Direct optimization of a vascular system, including topological changes, is used instead of simulating vessel growth. A good initial topology is found by extracting key information from a previously optimized model with less detail. This technique is used iteratively in a multi-level approach to create a globally optimized vascular system.

Global Constructive Optimization of Vascular Systems

Manfred Georg[1,2], **Tobias Preusser**[1,3], **Horst K. Hahn**[1]

[1] Fraunhofer MEVIS, Institute for Medical Image Computing, Universitätsallee 29,
   28359 Bremen, Germany.
[2] Media and Machines Laboratory, Computer Science and Engineering,
   Washington University, St. Louis, MO 63130-4899, USA.
[3] Jacobs University Bremen, Campus Ring 1, 28759 Bremen, Germany

Abstract   We present a framework for the construction of vascular systems based on optimality principles of theoretical physiology. Given the position and flow distribution of end points of a vascular system, we construct the topology and positions of internal nodes to complete the vascular system in a realistic manner. Optimization is driven by intravascular volume minimization with constraints derived from physiological principles. Direct optimization of a vascular system, including topological changes, is used instead of simulating vessel growth. A good initial topology is found by extracting key information from a previously optimized model with less detail. This technique is used iteratively in a multi-level approach to create a globally optimized vascular system.

Keywords

computational modeling, optimality principles, vascular anatomy, constrained constructive optimization.

1 Introduction

The understanding of vascular systems is important to many applications. Identifying vascular territories is crucial for providing resection proposals as well as for preoperatively estimating resection volumes and patient outcome [32, 4]. Surgery planning would directly benefit from better models of patient vascular systems [5]. The simulation of vascular remodeling and growth would be an asset in monitoring patient recovery after destructive surgery. Computer models can be used to create virtual CT scans useful for verifying vascular image analysis methods [18].

The problem is posed whether the geometry of a vascular system can be solely characterized as the minimum of a mathematical optimization principle. To this end, we define an appropriate optimization problem and cost function and develop an algorithm for its solution.

This formulation is motivated by the observation that natural systems exhibit optimality [25]. The main consideration in the optimization of a vascular system is the energy required in creating and
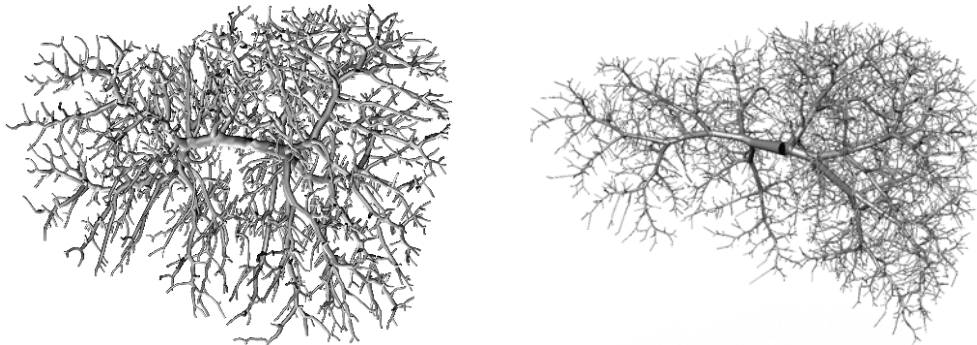
Fig. 1 Left: a vascular tree obtained in vitro from corrosion cast imaging [9]. Right: simulation result for a vascular system filling a liver shape obtained from CT in-vivo imaging.

maintaining the system [10, 22]. Specifically, the minimization of the intravascular volume has been identified as a driving design principle [13, 14].

The main contribution of this work is an algorithm for producing realistic vascular trees through the application of optimality criteria. Rather than growing these trees through the simulation of angiogenesis, we make the assumption that vascular systems, regardless of how they are formed, tend toward a state of optimality. Therefore, we directly model a fully formed vascular system without simulating its growth.

A vascular tree is approximated as a collection of connected, straight, cylindrical tubes where hydro-dynamic resistance is given by Hagen-Poiseuille's law assuming laminar flow of a perfect fluid. Various optimality criteria will constrain properties of the edges of this graph such as flow and radius. Our goal is to find a tree which minimizes the intravascular volume of the system while fulfilling the constraints. Not only are the positions of nodes within the tree optimized, but the topology of the tree itself is also optimized through the actions of splitting and merging branchings. We find that early topological choices in our optimization propagate through to the end, causing suboptimality. To remedy this prob-lem the coarse structure of optimized trees are used to create better initial trees for another round. This technique is repeated while maintaining progressively finer structures from the previous round until we arrive at our final result.

2 Related Work

A natural approach to modeling a vascular system is to simulate its growth through angiogenesis. Such a model of capillary systems was developed to generate realistic looking vascular patterns for surgical simulation [34]. However, it is too computationally expensive to be applied to macroscopic structures in three dimensions. Work modeling the growth, branching, and anastomosis [24] and explaining tree-like and net-like structures from the basic principles of activation, inhibition, and elongation have been developed but also suffer from a scaling problem [21].

Another approach uses a set of rules which explicitly encode optimality principles to create lung models deterministically from few predefined bifurcations and the shape of the organ [17, 35]. The rules steer volume partitioning, branching angles, radius and length ratios, and are applied recursively. Tawhai extends Kitaoka's work by introducing average dimensions and order distributions in order to statistically steer the branching process. Such models have been used in the study of lung dynamics and to create better lung phantoms [6, 7]. However, the rules must be carefully chosen to explicitly create realism. We wish to avoid this limitation by only indirectly influencing the shape of a vascular system through a more generic use of optimality principles. For example, we will not explicitly constrain branching angles or the degree of asymmetry of the vascular tree, but will still produce realistic results.

We take as a starting point Constrained Constructive Optimization (CCO) which builds a vascular system by iteratively adding terminal segments while following certain optimality criteria [27, 31, 30, 28, 29]. Our main modification to this approach is to optimize the entire vascular tree at once instead of only the branches around each segments as it is added.

Initial results for Global Constructive Optimization and their relation to fractal aspects of vascular systems were published by the authors in [8]. However, the details of this algorithm have not previously been published.

3 Modeling a Vascular System

3.1 Notation

We define a vascular system as a tree structure with node positions in two or three dimensions. Formally, this *tree* structure is defined as $\mathcal{G} := (\mathcal{N}, \mathcal{E})$ where $\mathcal{N}$ is a set of *nodes* which must contain a *root node* $r \in \mathcal{R}$ and a set of *leaf nodes* $\mathcal{L}$, and $\mathcal{E} \subset \mathcal{N} \times \mathcal{N}$ is a set of *directed edges* which form a connected, tree structure. The edge $e_j = (x_{j_1}, x_{j_2})$ is directed from x_{j_1} to x_{j_2} and the direction must always be away from the root node. Each edge has the following quantities associated with it: *length* defined as Euclidean distance between its source and destination nodes $l_j = \|x_{j_1} - x_{j_2}\|$, *radius* r_j, and *flow* f_j. The position of leaf nodes and the flow of their parent edge are provided by the user and may come from sources such as MRI perfusion imaging or doppler ultrasound. We denote the set of *neighbor edges* $\mathcal{B}_x$ of a node $x \in \mathcal{N}$ as the union of its *child edges* $\mathcal{A}_x = \{e \in \mathcal{E} \,|\, e = (x, y)\}$ and *parent edge* $\{e \in \mathcal{E} \,|\, e = (y, x)\}$. *Neighbor*
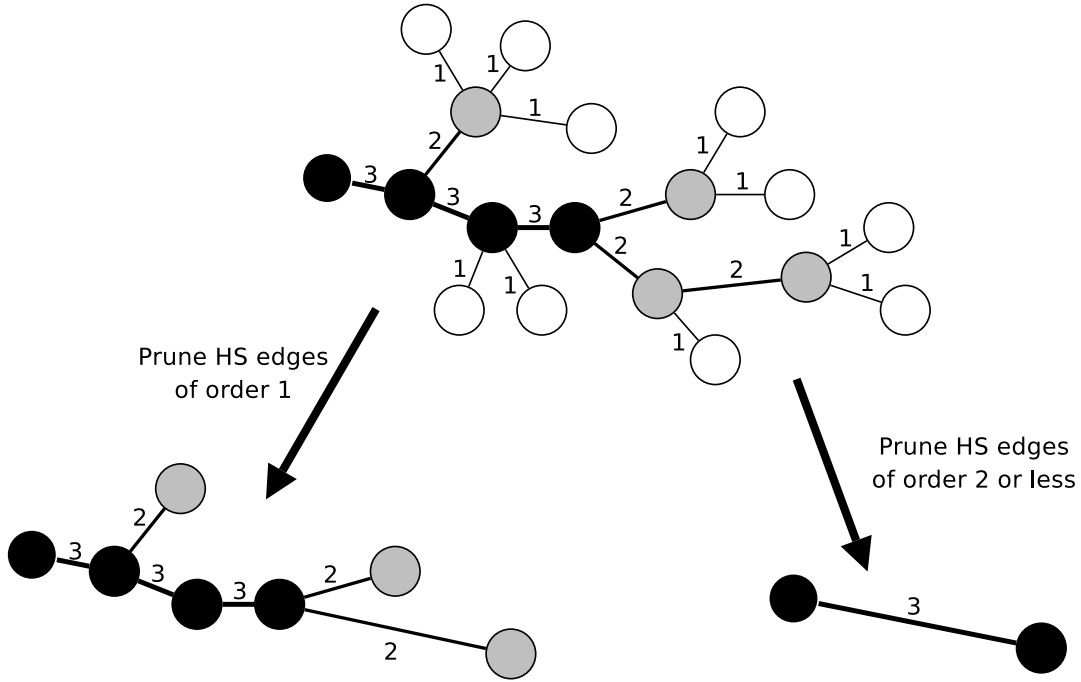
Fig. 2 An example tree structure with the Horton-Strahler order of each edge marked. The subtrees of a particular order can be extracted to obtain coarse level information about the tree.

nodes, *child nodes*, and *parent nodes* are defined as the nodes on the other end of their respective edges. We define the set of *terminal nodes* as $x \in \mathcal{L} \cup \mathcal{R}$ and the *branching points* as $x \in \mathcal{V} = \mathcal{N} \setminus (\mathcal{L} \cup \mathcal{R})$.

Horton-Strahler order: We use a graph based ordering scheme to define a hierarchy on the tree [11, 33]. To this end we introduce the Horton-Strahler order on the set of edges:

$$\mathrm{HS} : \mathcal{E} \to N \tag{1}$$

The edges directly connected to leaves are initialized with a Horton-Strahler (HS) order of 1. A non-leaf edge $(e = (x_k, x_j))$ is assigned the maximum HS order of its children $(h_e = \max_{e_c \in \mathcal{A}_{x_j}} \{\mathrm{HS}(e_c)\})$ unless there are two or more children with maximal HS order, in which case it is assigned the maximum plus 1.

$$\mathrm{HS}(e) = \begin{cases} 1 & \text{if } x_j \in \mathcal{L} \\ h_e + 1 & \text{if } \exists\, e_n \neq e_m \in \mathcal{A}_{x_j} \text{ such that } \mathrm{HS}(e_n) = \mathrm{HS}(e_m) = h_e \\ h_e & \text{otherwise} \end{cases} \tag{2}$$

The Horton-Strahler order of a node is defined as that of its parent edge. Figure 2 shows a tree structure with the Horton-Strahler order of each edge labeled.

3.2 Assumptions

We make several assumptions in our model. First, we assume a laminar, perfect fluid of constant viscosity flows through the vessel system. In reality, the Fåhræus-Lindqvist law states that blood has a lower effective viscosity when it flows through small capillaries [3]. However, we model blood vessels of diameter greater than 0.3 millimeters where blood viscosity is near constant. Additionally, we disregard the effects of angle of bifurcation and vessel curvature on pressure drops in the vascular system. Finally, we assume that our flow is steady, not pulsatile. There is literature suggesting that geometrically optimizing a vascular system is similar regardless of steady or pulsatile flow [1].

3.3 Physiological Considerations

Both the biochemical energy required to create and maintain blood, and the physical energy required to pump blood are costly. We assume that in the course of vascular growth these energy costs are minimized [13, 14]. The Hess-Murray law, which directly arises from this model, relates the flow through a vessel to its radius [10, 23].

$$f_j = \kappa\, r_j^\alpha \tag{3}$$

κ is a constant *flow coefficient* specific to each organ and vascular system and the *flow exponent* $\alpha \approx 3$ can be chosen to minimize specific properties such as shear stress as discussed in section 6.1.

Since flow must be conserved at a branching, for any node x the flow of the parent edge f_p must equal the sum of the flows of the child edges.

$$f_p = \sum_{e_j \in \mathcal{A}_x} f_j \tag{4}$$

In combination with (3) this constrains the radii of edges at a branching by the following power law.

$$(r_p)^\alpha = \sum_{e_j \in \mathcal{A}_{e_p}} (r_j)^\alpha \tag{5}$$

This equation generalizes beyond particular tissue types since κ is not present.

3.4 Definition of tree cost

Motivated by the minimization of intravascular volume we define a cost function for an edge $e \in \mathcal{E}$ as follows.

$$C(e) = r_e^\beta f_e^\gamma l_e \tag{6}$$

When $\beta = 2$ and $\gamma = 0$ this equation is the intravascular volume. Other values for β and γ are discussed in section 6.1.

The cost of a graph $\mathcal{G} = (\mathcal{N}, \mathcal{E})$ is the sum of the costs of all its edges:

$$C(\mathcal{G}) = \sum_{e \in \mathcal{E}} C(e) \tag{7}$$

3.5 The Global Optimization Problem

Consider the global optimization problem depicted in figure 3, in which we must find the best tree topology which provides fluid to the leaf nodes.

> *Given $\mathcal{L}$, $\mathcal{R}$, α, β, and prescribed flows and positions at each leaf node, find the tree $\mathcal{G} = (\mathcal{N}, \mathcal{E})$ with minimum cost that contains $\mathcal{L}, \mathcal{R} \subset \mathcal{N}$ as leaf and root nodes, respectively, and fulfills equation 3 and 4.*

The cost function of the tree is partially discrete due to topological choices and is non-convex. However, when considering a fixed topology, $C(\mathcal{G})$ is a function of the position of nodes and is convex. This follows from the cost of each edge $C(e)$ being convex when considered as a function of the position of the edge endpoints.
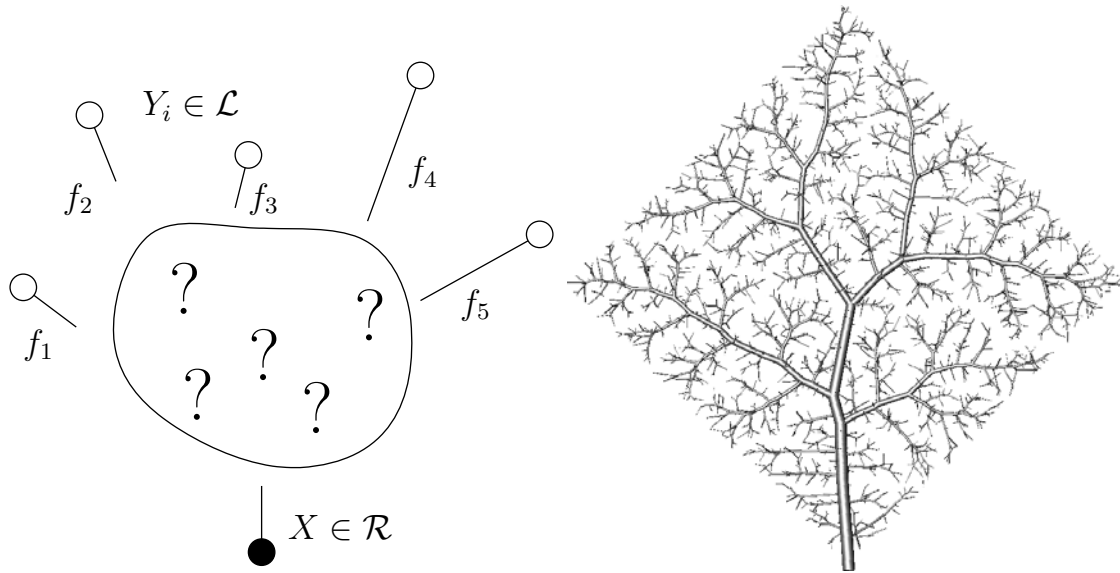
Fig. 3 Left: our goal is to create a realistic vascular structure given only the position and flow distribution of terminal nodes. Right: the resulting vascular structure created by our algorithm for a flat square. Note that despite the symmetric shape, the optimal configuration evolves to be asymmetric.
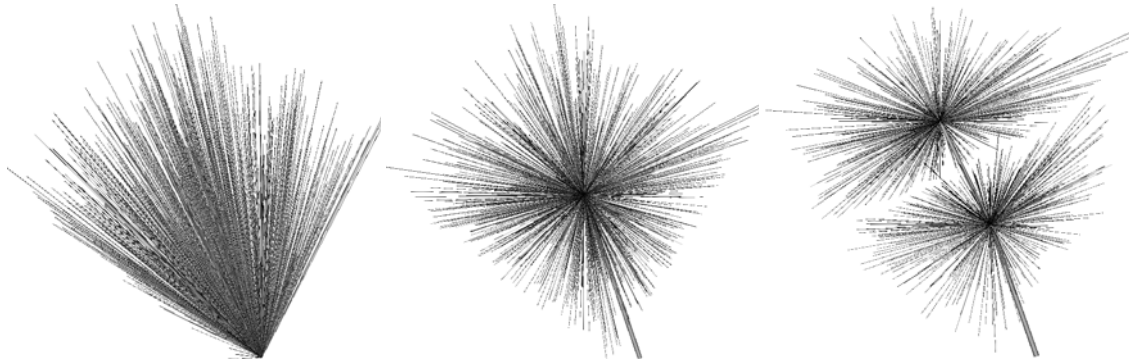
Fig. 4 One thousand leaf nodes are randomly positioned inside a cube and the root node is chosen near one of the corners. The process of optimization starts with a model where every edge connects a leaf node to the root node (left). The process of relaxation brings the large branching created by the initialization into the middle of the model (center). Splitting creates smaller nodes, which then relax to their own respective optimal positions (right).

4 Local Optimization Operators

We now introduce an algorithm which efficiently, numerically minimizes the above defined cost function, while respecting the desired constraints. This algorithm contains two main parts, which are presented in this section and section 5. The first part makes use of relaxation, merging, and splitting of the branchings, as seen in figure 4, to create an approximation of a vascular tree. This tree is then pruned and the leaf nodes are reconnected to their nearest neighbor to create the starting point for another round of optimization, as seen in figure 5. These two parts are repeated preserving progressively more detail in the pruning to arrive at a final vascular tree. Figure 6 provides a flow diagram of the algorithm.

In this section will manipulate the graph locally to create more optimal configurations. To measure this improvement, we define the local cost function for a node x as the sum of the cost of each of its neighboring edges ($\mathcal{B}_x$).

$$C_{\text{local}}(x) = \sum_{e \in \mathcal{B}_x} C(e) = \sum_{e=(a,b) \in \mathcal{B}_x} r_e^\beta \, \|a - b\| \tag{8}$$

When the node x is moved, the change in $C_{\text{local}}(x)$ is exactly the same as that in $C(\mathcal{G})$.

Fig. 5 A model, which has been optimized locally (left). The basic structure of this model when all edges of HS order 3 or less are removed (center). Initial state of the new model, which takes advantage of the old models structure (right).

4.1 Relaxation

We define the *pull force* for a set of edges S as their negative cost derivative.

$$F_S = - \sum_{e=(x,y_i) \in S} r_e^{\beta} \frac{y_i - x}{\|y_i - x\|} \; .$$ (9)

When $S = B_x$ this quantity is equal to the local cost derivative $\nabla C_{\text{local}}(x)$ and can be thought of as a force pulling the node to equilibrium, where the local cost is minimized. Note that the local cost derivative is solely dependent on the edge radii and not their lengths.

Since $C(\mathcal{G})$ is convex with fixed topology, we can use an optimization algorithm to find the global minimum of the cost function. We call the movement of all branching point positions to their globally minimal positions for a particular topology a *relaxation* of the tree. After relaxation, there is still a need for topological changes; namely, splitting and merging of nodes.

4.2 Merging

The process of merging involves joining two neighboring nodes and removing the edge that was between them. Merging should be done in a situation where relaxation would place a node at the same location as one of its neighboring nodes. Although it is possible to explicitly test for this condition, it is easier to merge nodes together when they are sufficiently close.

We test the length of each edge against the smallest of its neighbors $\{e^*\}$.

$$\frac{l_{e^*}}{l_e} \le \delta \qquad \forall e \in \mathcal{B}_x \setminus \{e^*\}$$ (10)

If this condition is fulfilled for the threshold $0 < \delta \ll 1$, we remove the edge and merge the two nodes which it connects. The connectivity of all involved edges is updated by connecting them all to the newly created node as shown in figure 7.

The special case of merging with a terminal node is handled by placing the branching node on top of the terminal node and allowing the pull force of the resulting zero length edge to pull against every direction. In this way, the branching node is anchored to the terminal node by the force of the zero length node.

4.3 Splitting

To decrease cost a single node with many edges is split into two nodes with fewer edges as shown in figure 8. A new node is created and connected to the old node and a subset of the edges of the original

Global Constructive Optimization
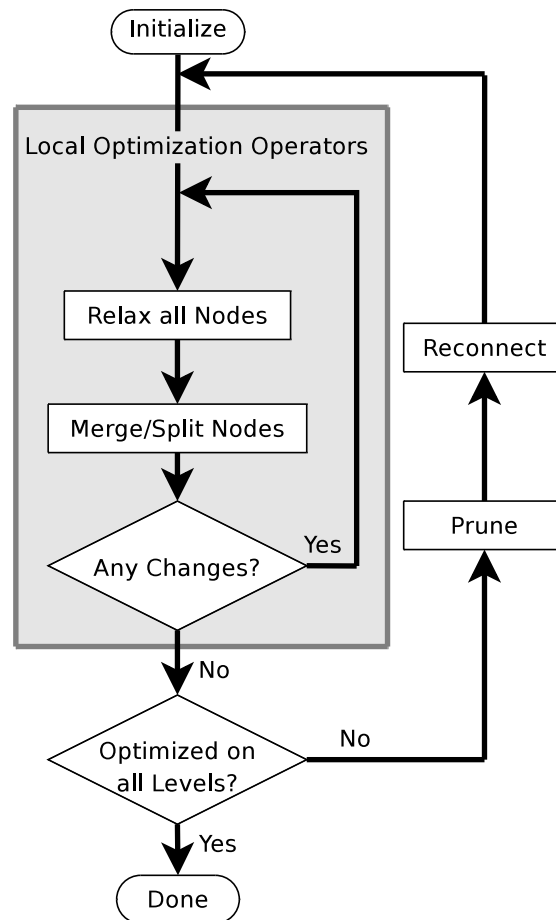
Fig. 6 A flow diagram of the complete algorithm. The inner loop optimizes a tree given an initial configuration which may contain coarse level topological information. The outer loop extracts coarse level tree structures and feeds them back into the optimizer.
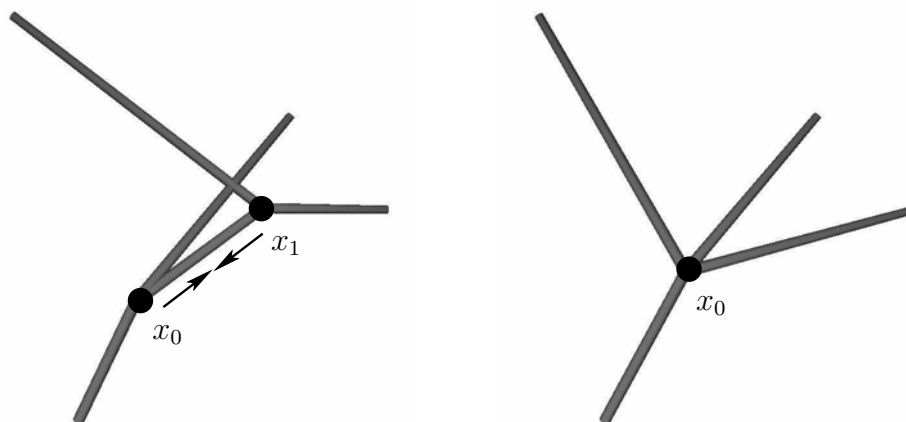
Fig. 7 Result of merge operation on a suboptimal configuration of two neighboring bifurcations. The two branchings are merged to form a trifurcation: pre-merge (left) and post-merge configuration (right).
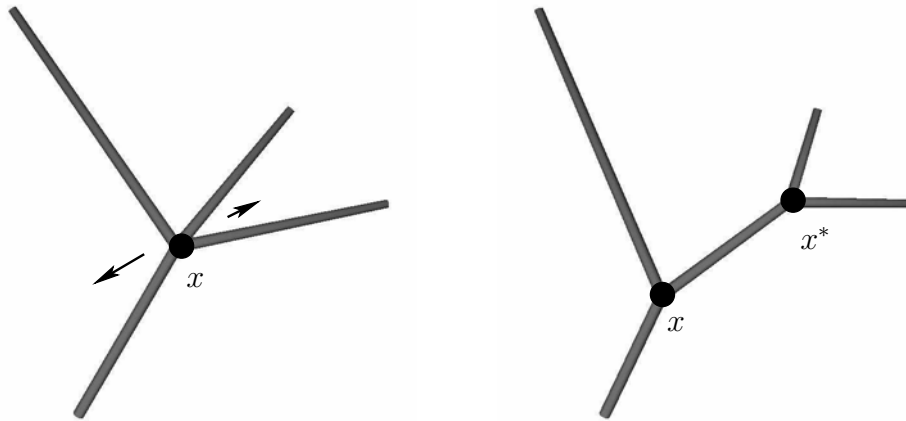
Fig. 8 The suboptimal branching is split into two bifurcations: pre-split (left) and post-split configuration (right). The pre-split corresponds to the post-merge configuration of Fig. 7 after relaxation.

node $S \subset \mathcal{B}_x$ are moved to be connected to the new node instead. The radius of the new edge v connecting the nodes is given by the radius law given in equation 5.

$$r_v = \left(\sum_{e \in S} r_e^\alpha \right)^{1/\alpha} \tag{11}$$

To find the optimal edges to move to the new node, we compare the pull force of the set of edges to be moved to the pull force of the edge that would exist if all the edges were aggregated into a single edge.

$$\sigma(S) = \|F_S\| - r_v^\beta \qquad \text{if } F_S \neq 0 \tag{12}$$

We define the difference between these two quantities $\sigma(S)$ as the *rupture strength*. This quantity indicates the gain from aggregating the edges in S into one edge.

It is computationally expensive to search all sets of edges S to split into a new node. Instead, we perform a search by first finding the set S_2 with two edges which maximizes rupture strength. We then iteratively find the sets S_n with highest rupture strength which contain all the edges in S_{n-1}. The set we thus encounter with the highest rupture strength is chosen as the set of edges to split onto another node. We have empirically found that this algorithm finds the absolute best split in all cases we have been able to verify.

5 Global Constructive Optimization

5.1 Initialization

Initially, we generate the set of leaf nodes $\mathcal{L}$ by either filling a grid or by picking uniformly random points within the volume. We have found that either method creates similar large scale branching structure, as can be seen in figure 9. The location of the root node is chosen manually. To initialize, we create edges that connect the root node $x \in \mathcal{R}$ directly to each of the leaf nodes as shown in figure 4.

The flows at each of the leaves is initialized to a constant value. In the simplest case, this value is identical for all leaves; however, any flow distribution, such as one derived from physiological data, can be chosen. Equation 3 is used to initialize the radius of all edges.

5.2 Hierarchical Topology Readjustment

Branchings rarely merge together after they have been split apart. This can lead to early decisions in the branching structure being preserved throughout the optimization process as shown in figure 10. We address this problem with *hierarchical-iterations*, where the coarse structure of an optimized tree is used to initialize a new tree which will have more optimal fine structures.
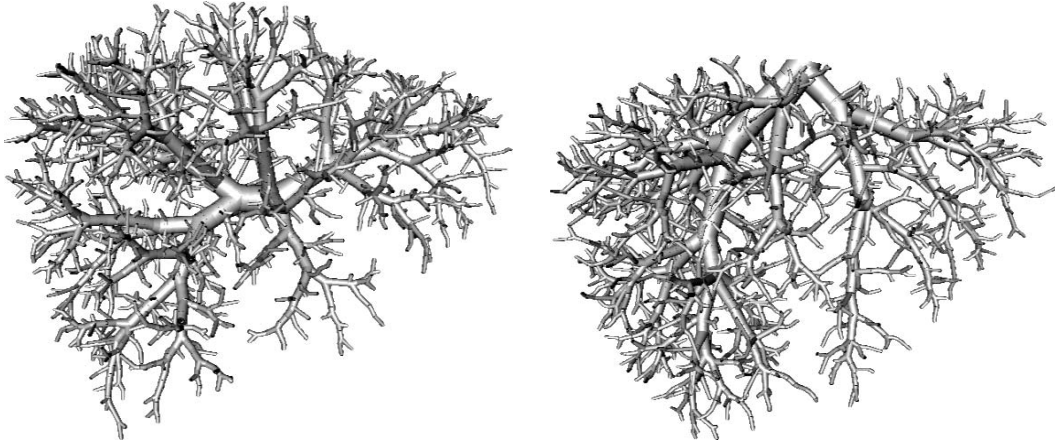
Fig. 9 Result for shape of a real liver, similar to a portal (left) and a hepatic venous tree (right). Identical optimization parameters and organ shape were used for both images. The only differences are the initial root position (manually chosen) and leaf positions (left: square grid, right: random), and a slightly different viewpoint.

Fig. 10 Large splitting planes are the result of early divisions: Left: First split in an optimization with corresponding splitting plane. Center: The resulting splitting plane can be clearly discerned at the same position after local optimization (arrows). Right: Same model after this problem has been resolved through the use of hierarchical-iterations.

A pruned tree $\mathcal{G}^\ell = (\mathcal{N}^\ell, \mathcal{E}^\ell)$ is created from $\mathcal{G}$ by removing all edges with Horton-Strahler order smaller than some threshold.

$$\begin{aligned} \mathcal{E}^\ell &= \{e \in \mathcal{E} \mid \mathrm{HS}(e) \geq \ell\} \\ \mathcal{N}^\ell &= \{x \in \mathcal{N} \mid (x,y) \in \mathcal{E}^\ell \text{ or } (y,x) \in \mathcal{E}^\ell\} \end{aligned} \tag{13}$$

This step creates freedom of movement by removing minor bifurcations which anchor the tree to a local minimum. We *reconnect* all the leaf nodes, which were removed in the pruning stage, to the nearest node in the pruned tree. The new tree $\mathcal{G}' = (\mathcal{N}', \mathcal{E}')$ is created from the pruned tree $\mathcal{G}^\ell$ and the leaf nodes $\mathcal{L}$.

$$\begin{aligned} \mathcal{N}' &= \mathcal{N}^\ell \cup \mathcal{L} \\ \mathcal{E}' &= \mathcal{E}^\ell \cup \{e = (x,y) \mid y \in \mathcal{L}, x \in \mathcal{N}^\ell, \ \|y - x\| \leq \|y - a\| \forall a \in \mathcal{N}^\ell\} \end{aligned} \tag{14}$$

In this way, a new tree is created with larger branchings than the original tree as shown in figure 5. This tree is optimized to produce a new tree with better global branching structure.

In each hierarchical-iteration we use the information from progressively finer hierarchical levels. The first hierarchical-iteration is performed on a tree with $\ell_{\max}$ hierarchical levels. The $\ell_{\max} - 1$ smallest levels are pruned away leaving only the coarsest skeletal structure. The leaf nodes are reconnected to this skeletal structure, and the resulting tree is optimized. This process is repeated while preserving one more hierarchical level then the previous iteration, until all the hierarchical levels have been used. Figure 11 shows the global cost decreasing during optimization. Each spike coincides with a new pruning step on progressively smaller hierarchical levels.
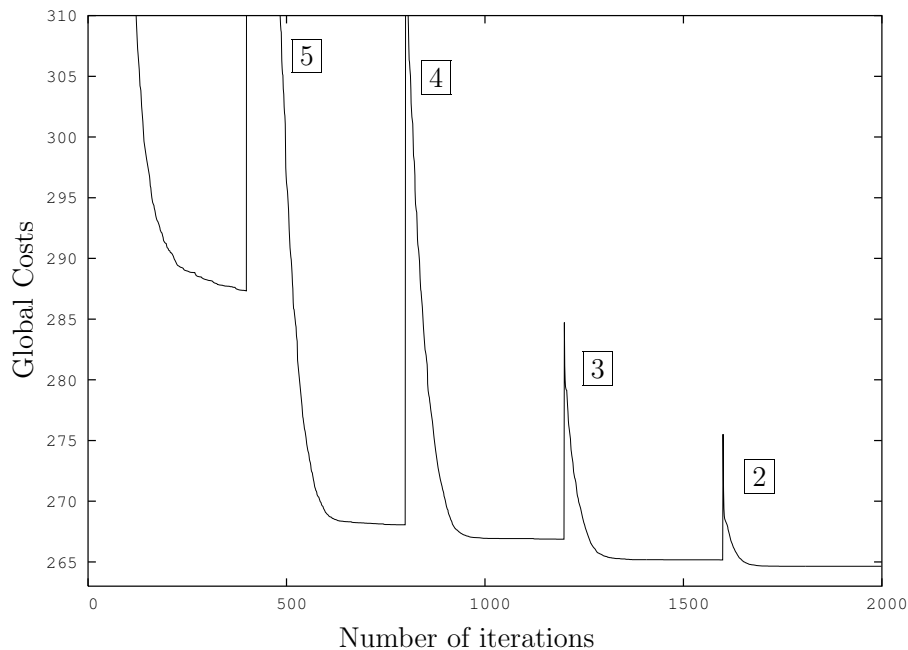
Fig. 11 The evolution of the global costs versus the number of gradient evaluations is shown for the hierarchical optimization algorithm. The boxed numbers near the spikes show the smallest Horton-Strahler level which was preserved in the pruned tree.

5.3 Convergence and Complexity

The algorithm will converge to a local minimum of the cost function, since merging and splitting will only be performed when they will decrease cost, and the relaxation step finds the minimum within a fixed topology.

The computational complexity of the algorithm has two main components. First, finding the splitting edges S of a branching has complexity $O(N^2)$ where N is the number of edges in the branching. Finding the set S_2 has complexity $O(N^2)$ and each of the $N-2$ additional sets S_n require a scan of the edges for a total of $O(N^2)$. For the initial branching all N edges are in one branching, this is the most time consuming branching. The second major component of the complexity of the algorithm is in the relaxation step. Each computation of the gradient requires a scan through the edges of the graph, and must be done for each of k iterations of the optimization algorithm. The merging steps do not require any additional complexity since the length of edges must be computed in the relaxation step anyway. Therefore the complexity of each pruning of a tree is $O(N^2 + k\,N)$. In the worst case the highest Horton-Strahler number for an edge is on the order of $O(\log(N))$ so the complete complexity of Global Constructive Optimization is $O(N^2 \log(N) + k\,N \log(N))$.

We were able to completely optimize trees containing 1,000 nodes in approximately 3 minutes of computation time on a Pentium III, 800 MHz, with 256 MB of RAM. Trees with 12,000 nodes were optimized in a couple hours.

6 Discussion and Future Work

6.1 Physiological Parameters

In the works of Hess and Murray, the *flow exponent* α was fixed at a value of 3.0 which minimizes shear stress on the vessel walls [28]. Other values of α are motivated by minimizing different quantities. For example, a value of 2.55 will minimize wave reflection in pulsatile blood flow [1] and the optimal α when considering non-laminar flows varies between 2.33 for a fully turbulent flow and 3.0 for a fully laminar flow [37, 26]. Since results have already been published for $\alpha = 3.0$ we have used this value throughout the paper [22, 13, 28].

The choice of β and γ can be set to minimize specific quantities such as intravascular volume ($\beta = 2, \gamma = 0$), vascular surface area ($\beta = 1, \gamma = 0$), surface forces ($\beta = -2, \gamma = 1$), or work ($\beta = -4, \gamma = 2$) [26, 39, 40]. In this paper we have minimized intrevascular volume ($\beta = 2, \gamma = 0$).

Several studies have verified scaling laws and parameter values in real vascular systems. Morphometric data has been used to determine parameters of scaling laws in specific organs of various species [15, 2]. The contraction of the vascular smooth muscles has been used to explain volume differences between the initial and terminal generations of a vascular system from an optimality perspective [16].

Vascular systems exhibit several fractal properties such as volume filling and scale invariance [19]. Fractal geometry as a biological design principle was put forth in [38]. Specifically, fractal dimension can be related to the free parameters in optimality equations and the asymmetry exhibited in the branchings of the vascular system [36, 12].

6.2 Complementary Trees

A vascular system is composed of more than one vascular tree connected through the capillaries. In our method this could be modeled by having multiple root nodes which connect to the same set of leaf nodes. The two main challenges to extending our method in this way are that collisions between trees must be dealt with and that all paths between roots must have consistent pressure drops. A technique similar to CCO has been used to create a vascular system comprised of two complementary vascular trees [18]. In this model, collisions between the two trees are dealt with explicitly. In general, the radius of edges can be adjusted to create consistent pressure drops, at the expense of violating the radius law.

It has been found that the hydrodynamic pressure drops from the root to the vascular endpoints exhibit a wide distribution [28]. Given this, the combination of a short perfusion path with a long drainage path, or vice versa, requires less total intravascular volume than any other combination. We therefore conjecture that optimization with regards to pressure and flow causes opposing vascular trees to naturally separate.

The natural separation between complementary trees makes it less likely that a trauma to the organ will cause the vascular trees to connect causing a short circuit. This line of reasoning has been investigated by B. Mauroy et al. for the bronchial system [20]. Following their arguments, "the design of bronchial trees must be provided with a safety factor and the capacity for regulating airway calibre", without risking very large variations in air supply. It is a fundamental question, whether a corresponding safety argument applies to blood vessels.

6.3 Medical Applications and Evaluation

Comparing the generated models for the shape of the human liver with vascular information obtained from corrosion casts reveals a striking similarity in terms of gross vascular anatomy, branching patterns, and asymmetry [9]. Quantitative results on scaling and branching properties, such as radius and length ratios, show a good correspondence.

A potential approach to evaluate our model is to use in vivo data as an initialization for the global optimization procedure and to quantify the differences between the initial and final configuration. This would lead to an estimation of the predictive power of optimality in vascular systems.

7 Conclusion

We have presented an algorithm for creating vascular trees. Instead of simulating the growth of a vascular system, we directly apply optimality criteria to find an optimal tree structure. Initial stages in our algorithm produce suboptimal global structure which cannot be corrected by considering the tree locally. We therefore use the coarse structure of a previously optimized tree to initialize a new tree. This technique is iterated while using progressively finer structures until we arrive at our final result. The vascular trees found using our method exhibit realism both in the properties we have explicitly optimized and in secondary properties such as branching angle and asymmetry. In conclusion, we find that optimality criteria can be used to create realistic vascular trees even when the growth process is not explicitly simulated.

Acknowledgments

References

1. Arts, T., Kruger, R. T. I., van Gerven, W., Lambregts, J. A. C., and Reneman, R. S. 1979. Propagation velocity and reflection of pressure waves in the canine coronary artery. Am. J. Physiol. 237:H469–H474.

2. Choy, J. S. and Kassab, G. S. 2008. Scaling of myocardial mass to flow and morphometry of coronary arteries. Applied Physiology 104:1281–1286.

3. Fåhræus, R. and Lindqvist, T. 1931. The viscosity of the blood in narrow capillary tubes. J. Physiol. 96:562–568.

4. Fasel, J. H. D., Gailloud, P., Grossholz, M., Bidaut, L., Probst, P., and Terrier, F. 1996. Relationship between intrahepatic vessels and computer-generated hepatic scissurae: An in vitro assay. Surg. Radiol. Anat. 18:43–46.

5. Fasel, J. H. D., Selle, D., Evertsz, C. J. G., Terrier, F., Peitgen, H.-O., and Gailloud, P. 1998. Segmental anatomy of the liver: Poor correlation with CT. Radiology 206:151–155.

6. Felici, M., Filoche, M., and Sapoval, B. 2004. Renormalized random walk study of oxygen absorption in the human lung. Phys. Rev. Lett. 92:068101.

7. Garrity, J., Segars, W., Knisley, S., and Tsui, B., 2002. Development of a dynamic model for the lung lobes and airway tree in the ncat phantom. volume 3, Pages 1858–1862.

8. Hahn, H., Georg, M., and Peitgen, H.-O. 2005. Fractal aspects of three-dimensional vascular constructive optimization. Fractals in Biology and Medicine 4:55–66.

9. Hahn, H. K., Evertsz, C. J. G., Fasel, J. H. D., and Peitgen, H.-O. 2003. Fractal properties, segment anatomy, and interdependence of the human portal vein and the hepatic vein in 3D. Fractals 11:53–62.

10. Hess, W. R. 1914. Das Prinzip des kleinsten Kraftverbrauchs im Dienste hämodynamischer Forschung. Archiv Anat. Physiol. 1914:1–62.

11. Horton, R. E. 1945. Erosional development of streams and their drainiage basins; Hydrophysical approach to quantitative morphology. Bull. Geol. Soc. Am. 56:275–370.

12. Kamiya, A. and Takahashi, T. 2007. Quantitative assesments of morphological and functional propertios of biological trees based on their fractal nature. Applied Physiology 102:2315–2323.

13. Kamiya, A. and Togawa, T. 1972. Optimal branching structure of the vascular tree. Bull. Math. Biophysics 34:431–438.

14. Kamiya, A. and Togawa, T. 1974. Theoretical relationship between the optimal models of the vascular tree. Bull. Math. Biol. 36:311–323.

15. Kassab, G. S. 2005. Scaling laws of vascular trees: of form and function. Applied Physiology 290:894–903.

16. Khanin, M. A. and Bukharov, I. B. 2003. Optimal structure of the circulatory system: Influence of the energetics of vascular smooth muscles. Optimization Theory and Applications 116:347–357.

17. Kitaoka, H., Takaki, R., and Suki, B. 1999. A three-dimensional model of the human airway tree. J. Appl. Physiol. 87:2207–2217.

18. Kretowski, M., Rolland, Y., Bézy-Wendling, J., and Coatrieux, J.-L. 2003. Physiologically based modeling of 3-D vascular networks and ct scan angiography. IEEE Trans. on Med. Imaging 22:248–257.

19. Mandelbrot, B. B., 1982. The Fractal Geometry of Nature. W. H. Freeman, San Francisco, CA.

20. Mauroy, B., Filoche, M., Weibel, E. R., and Sapoval, B. 2004. An optimal bronchial tree may be dangerous. Nature 427:633–636.

21. Meinhardt, H., 1982. Models of Biological Pattern Formation. Academic Press, London.

22. Murray, C. D. 1926. The physiological principle of minimum work applied to the angle of branching of arteries. J. Gen. Phys. 9:835–841.

23. Murray, C. D. 1926. The physiological principle of minimum work. I. The vascular system and the cost of blood volume. Proc. Natl. Acad. Sci. U.S.A. 12:207–214.

24. Nekka, F., Kyriacos, S., Kerrigan, C., and Cartilier, L. 1996. A model of growing vascular structures. Bull. Math. Biol. 58:409–424.

25. Rosen, R., 1967. Optimality Principles in Biology. Butterworths, London.

26. Roy, A. G. and Woldenberg, M. J. 1982. A generalization of the optimal models of arterial branching. Bull. Math. Biol. 44:349–360.

27. Schreiner, W. 1993. Computer generation of complex arterial tree models. Journal Biomedical Engineering 15:148–150.

28. Schreiner, W., Karch, R., Neumann, M., Neumann, F., Roedler, S. M., and Heinze, G. 2003. Heterogeneous perfusion is a consequence of uniform shear stress in optimized arterial tree models. J. Theor. Biol. 220:285–301.

29. Schreiner, W., Karch, R., Neumann, M., Neumann, F., Szawlowski, P., and Roedler, S. 2006. Optimized arterial trees supplying hollow organs. Medical Engineering and Physics 28:416–429.

30. Schreiner, W., Neumann, F., Karch, R., Neumann, M., Roedler, S. M., and End, A. 1999. Shear stress distribution in arterial tree models, generated by constrained constructive optimization. J. Theor. Biol. 198:27–45.

31. Schreiner, W., Neumann, F., Neumann, M., End, A., and Müller, M. R. 1996. Structural quantification and bifurcation symmetry in arterial tree models generated by constrained constructive optimization. J. Theor. Biol. 180:161–174.

32. Selle, D., Preim, B., Schenk, A., and Peitgen, H.-O. 2002. Analysis of vasculature for liver surgical planning. IEEE Trans. Med. Imaging. 21:1344–1357.

33. Strahler, A. N. 1957. Quantitative analysis of watershed geomorphology. Am. Geophys. Union Trans. 38:913–920.

34. Szczerba, D. and Székely, G., 2002. Macroscopic modeling of vascular systems. in Proc. MICCAI, Pages 284–292. Springer, Berlin.

35. Tawhai, M. H., Pullan, A. J., and Hunter, P. J. 2000. Generation of an anatomically based three-dimensional model of the conducting airways. Ann. Biomed. Eng. 28:793–802.

36. Turcotte, D. L., Pelletier, J. D., and Newman, W. I. 1998. Networks with side branching in biology. J. Theor. Biol. 193.

37. Uylings, H. B. M. 1977. Optimization of diameters and bifurcation angles in lung and vascular tree structures. Bull. Math. Biol. 39:509–520.

38. Weibel, E. R. 1991. Fractal geometry: A design principle for living organisms. Am. J. Physiol. 261:L361–L369.

39. Zamir, M. 1976. The role of shear forces in arterial branching. J. Gen. Physiol. 67:213–222.

40. Zhou, Y., Kassab, G. S., and Molloi, S. 1999. On the design of the coronary arterial tree: A generalization of Murray's law. Phys. Med. Biol. 44:2929–2945.